Applied Catalysis B: Environmental 236 (2018) 294–303

Contents lists available at ScienceDirect

Applied Catalysis B: Environmental

journal homepage: www.elsevier.com/locate/apcatb

Influence of surface-functionalized multi-walled carbon nanotubes on CdS nanohybrids for effective photocatalytic hydrogen production

Madhusudana Gopannagari, D. Praveen Kumar, Hanbit Park, Eun Hwa Kim, Palagiri Bhavani, D. Amaranatha Reddy, Tae Kyu Kim*

Department of Chemistry and Chemical Institute for Functional Materials, Pusan National University, Busan 46241, Republic of Korea

ARTICLE INFO

Keywords:
Functionalized carbon nanotubes
CdS nanorods
Surface-Interaction
Water-Splitting
Hydrogen

ABSTRACT

Carbon nanotubes (CNTs) have enormous potential for application due to their extreme hydrophobicity. Further, their physico-chemical properties can be modified by surface functionalization. Acid functionalization of CNTs is one of the basic methodology for modification of their electro-chemical properties, resolving the poor dispersion capability, and improving the surface-active sites to enhance the photocatalytic efficiency. However, the role of surface functional groups on CNTs for water-splitting in association with CdS photocatalysts has not yet been sufficiently explored. Hence, in the present study, we report the influence of surface-functionalized CNT-metal nanoparticle (NP) hybrids attached to CdS nanorods for enhanced photocatalytic H_2 production. Significant improvement in photocatalytic H_2 production was observed for binary composites such as amine (Nf-), sulfonic (Sf-), and ascorbic acid (Af-) functionalized CNTs and CdS nanorods. Furthermore, the secondary functionalized Af-CNTs were incorporated with metal NPs and the photocatalytic activity was significantly improved in ternary metal-Af-CNT/CdS nanohybrids. Among the metal NPs, Pt- incorporated into Af-CNTs and its CdS nanohybrid led to the highest rate of H_2 production (120.1 mmol h^{-1} g^{-1}), corresponding to a 48-fold enhancement relative to that of pure CdS. The enhanced rate of H_2 production is attributed to the influence of the surface functional groups on the CNTs. The intimate interfacial contact between CdS, functionalized CNTs and metal NPs leads to enhanced photocatalytic performance, as a contributing factor for improving photogenerated charge separation and transportation. Moreover, the functional groups on CNTs (Pt-Af-CNT/CdS) led to obvious advantages, such as enhanced photoactivity and photostability of CdS for H_2 production. The photocatalytic performance of these nanohybrids was found to be highly influenced by the surface states of the CNTs, suggesting the importance of surface treatment of materials for H_2 evolution.

1. Introduction

The discovery of carbon nanotubes (CNTs) has proven to be an exceptional breakthrough for advancing the use of nanomaterials in science and technology and offers new opportunities for the design of effectual functional materials for numerous applications [1–3]. These one-dimensional structured CNTs possess a large surface-area, excellent physicochemical and electrical properties which are especially beneficial for electrochemical applications, and several approaches have shown their advantages for electrochemical hydrogen evolution [4–6]. Moreover, CNT nanoframeworks can act as templates for the preparation of metal-based catalytic interfaces by enhancing the active surface area, while the phase boundaries may further enhance the electrocatalytic efficiency [7]. However, the strong van der Waals interactions and the hydrophobicity of CNTs lead to poor dispersion in solvents and this insufficient chemical compatibility greatly limits the range of applications of CNTs [8,9].

Covalent surface functionalization is fundamental way used to overcome these problems. Surface functionalization can enhance the solubility of CNTs in various solvents and facilitate the production of novel hybrid materials for a potentially wide range of applications [9]. Traditional acid functionalization is used to introduce carboxyl and carbonyl functional groups that may enhance the solubility of CNTs [10–13]. Besides, the surface chemical functional groups of CNTs are not only beneficial for conferring hydrophilicity to the surface and for interfacial contact between metals and semiconductors, but also induce the synergetic effects to improve the electrochemical and photocatalytic efficiency [14,15]. These pre-treated CNTs can introduce a substantial number of surface functional groups which can act as an anchoring sites for reagents and provide additional reaction centers [16–18]. However,

* Corresponding author.
E-mail address: tkkim@pusan.ac.kr (T.K. Kim).

https://doi.org/10.1016/j.apcatb.2018.05.009
Received 4 February 2018; Received in revised form 2 May 2018; Accepted 3 May 2018
Available online 04 May 2018
0926-3373/ © 2018 Elsevier B.V. All rights reserved.

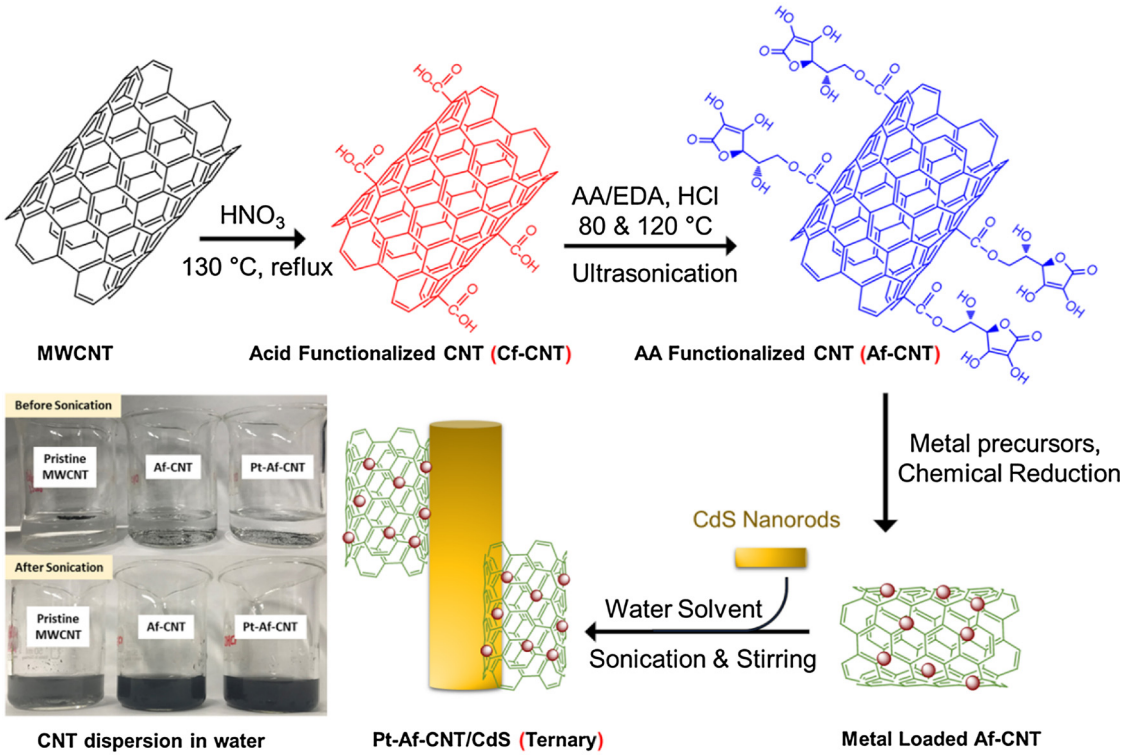

Fig. 1. Schematic illustration of the synthesis of AA-functionalized CNTs, Pt nanoparticle deposition, and CdS nanohybrids. Digital pictures show the dispersion of CNTs, Af-CNT, Pt-Af-CNTs before and after sonication.

the disadvantages of these acid functionalizations are that the structure and original properties of CNTs that could restricts the charge transfer properties, thus modifying the CNTs with gentle alternation of the intrinsic structural and electronic properties has become a major challenge [19]. In this regard, acid-functionalized CNTs have been extensively exploited for further chemical functionalization with metals and chemical compounds such as inorganic compounds, polymers, vitamins, biomolecules, and for self-assembly of CNTs into device structures [20–25]. The secondary surface functionalization can be achieved to effectively enhance the physico-chemical, electrical and optical properties, such the adsorption and surficial active sites of the CNTs that could advantage for electrochemical and photocatalytic applications [26]. Such secondary functionalization of CNTs have not yet been explored for electrocatalytic or photocatalytic applications [27–29] and needs to be investigated.

Cadmium sulfide (CdS) has been widely studied as photocatalyst due its high visible-light absorption ability and affords great potential for solar light applications. However, its rapid photo-induced hole/electron pair recombination leads to extremely low activity and poor stability [30]. Previously, several studies have assessed the influences of CNTs and acid-treated CNTs as electron acceptors in photocatalysts. For example, Robel et al. utilized the single-walled CNT (SWCNT) and Cao et al. employed multi-walled CNT (MWCNT) as electron accepting and charge transport channels in CdS nanosystems for the development of a CNTs/CdS composites [31,32]. Kim et al. studied the acid-treated (primary functionalized) CNTs as a light harvesting material and conducting channel for connecting CdS to Pt nanoparticles to produce a catalyst for proton/water reduction [33]. Recently, Li et al. reported the structural integrity of primary functionalized double-walled CNTs (DWCNTs) as an electron mediator between CdS nanoparticles and mono-layered MoS_2 composites for photocatalytic H_2 production [34]. Theoretically, Feng et al. showed the crucial role of surface-functionalized carbon dots (with −OH, −CHO, and −COOH functional groups) in water-splitting reactions [35]. Therefore, the secondary functionalization of CNT can deteriorate the photocatalytic performance.

In this regard, the secondary functionalization of CNTs with biological molecules, such as ascorbic acid (AA) [36,37] for photocatalytic applications holds a great promise. This AA used for functionalization, as an eco-friendly and bio-safe material, is widely used for functionalization of CNTs to improve the hydrophilic nature [21]. Functionalization with AA advance the dispersion of CNTs in aqueous solutions and improves the interfacial interaction and compatibility between the resulting AA-CNTs and polymer matrices [21,38]. Thus, anchoring AA functional groups to pre-treated CNTs functional groups provides electron conducting channels that could affects the surface interactions in CdS-based photocatalysts. This can, in turn, improve the charge separation and transport property, leading to greater photocatalytic activity. Moreover, introducing metal nanoparticles into these secondary functionalized CNTs could produce effective charge interactions by increasing the H^+/H_2 actives sites on the surface of the CdS photocatalyst [33].

Herein, we introduce secondary surface functional groups into the CNTs and exploit their interaction with metal nanoparticles on CdS nanorods for photocatalytic H_2 production. To the best of our knowledge, this is the first report to assess the role of multiple functional groups of CNTs for photocatalytic applications. This study presents the two-step functionalization of CNTs for tethering CNTs with carboxylic (Cf-), sulfonic (Sf-), amine (Nf-), and AA (Af-) functional groups (binary fCNT/CdS) on CdS nanorods. The interaction of these tethered CNTs with metal nanoparticles (M: Pt, Ru, Pd, Ni, Ag, Cu), their decoration on the surface of fCNTs with CdS nanohybrids (ternary M-CNT/CdS), and their novel application to H_2 production via photocatalytic water splitting are also explored. Compared to basic fCNT-CdS based H_2 production via water splitting, the developed composite exhibits the highest photocatalytic H_2 production and QE reported, as far as we are aware (Table S1).

2. Results and discussion

2.1. Synthesis process

For synthesis of the Pt-Af-CNT/CdS photocatalyst, primary surface functionalized MWCNTs were first synthesized by acid refluxing at the desired temperature to introduce carboxyl functional groups onto the surface of the CNTs (Cf-CNTs). This chemical modification of the CNT surface can provide improved compatibility with the reagents and provides an avenue for further chemical modification. Secondary surface functionalization of the CNTs was achieved by amidation and sulfonation; the detailed experimental process is illustrated in Fig. S1. Furthermore, AA-functionalized CNTs were synthesized via simple heating followed by ultrasonication of AA with the Cf-CNTs, where the chemical process involved slightly modified esterification reactions [38]. In this functionalization process, Af-CNTs were formed by esterification of the AA molecules with the carboxyl acid group on the surface of the Cf-CNTs, as shown in Fig. 1. Additionally, metal nanoparticles were loaded onto the surface of the Af-CNTs by sequential adsorption and chemical reduction. The M-NP-loaded Af-CNTs (as a ternary nanohybrid) and those without M-NPs (as binary nanocomposite materials) were allowed to interact with the CdS nanorods via a simple sonication and stirring process. Fig. 1 signifies the dispersion of pristine CNTs in water as hydrophobic nature, whereas, in Af-CNT and Pt-Af-CNTs (hydrophilic) dispersed well before adding the CdS nanorods. The interfacial interactions and dispersion of the Af-CNT and M-Af-CNT materials were greatly improved due to the presence of the functional groups on the surfaces, and these surfaces interacted strongly with the CdS nanorods, which may be beneficial for enhancing the light absorption and photocatalytic efficiency.

2.2. FT-IR analysis

The surface chemical identity of the functionalized CNTs were characterized by FTIR analysis, as displayed in Fig. 2(a and b). The functional groups of the Cf-CNT were confirmed by the presence of the C—O stretching band at 1072 cm^{-1}, carboxyl C═O stretching at 1634 cm^{-1}, and C—H and O—H bands at 2927 cm^{-1} and 3435 cm^{-1}, respectively. Secondary functionalization of the Nf-, Sf-, and Af-CNTs was successfully confirmed based on observation of the amine signals of the Nf-CNTs at 1089 cm^{-1}, 1617 cm^{-1}, and 2924 cm^{-1}, corresponding to C—N, N—H bending, and C—H stretching, respectively. The sulfonic groups of Sf-CNT were indicated by bands at 1230 cm^{-1} and 1736 cm^{-1}, ascribed to S═O and C═O groups, respectively [39]. The spectral analysis data indicated the successful functionalization of AA onto Cf-CNT surfaces through esterification and were compared with pristine MWCNTs and ascorbic acid compound. The organic moieties of the Pt-Af-CNTs and Af-CNTs were characterized by absorptions of the O—H groups at 3424 cm^{-1} and typical peaks around 2852 − 2027 cm^{-1}, ascribed to aliphatic sp^3 C—H groups [38,40]. The characteristic ascorbic acid peaks of the O—C═O (ester) group at 1732 cm^{-1} and 1126 cm^{-1} are attributed to the C—O vibrations shown in Fig. 2(b). It is evident that functionalization of the CNTs with AA via reaction with the carboxylic acid moiety allows direct attachment by an ester bond [38]. On the other hand, Pt nanoparticles deposited Af-CNTs ester (C—O) features, peak shifted to lower frequency at 1094 cm^{-1}, indicative of strong interaction of the Pt nanoparticles with the ester O [41]. The presence of the AA-functionalized CNTs on CdS improved the activity, and the Pt nanoparticle-loaded Af-CNT exhibited enhanced photocatalytic H_2 production. Additional surface functional groups lead to adequate interactions with the photocatalyst and metal nanoparticles, which in turn enhances the charge transfer and surface active sites.

2.3. Raman and structural analysis

Fig. 2(c) shows the Raman spectra of the pure CNTs, along with those of the functionalized CNTs. The characteristic peaks of the pristine CNTs were observed at 1348 cm^{-1} and 1577 cm^{-1}, corresponding to the D- and G-band, respectively. It is well known that the D-band originates mainly from typical defects or disorder in the sp^2-hybridized carbon [42], whereas the other characteristic feature of the graphitic layers, the G-band, is induced by tangential C—C stretching vibrations corresponding to the high frequency E_{2g} first order mode [43]. The secondary functionalized Af-CNTs showed a slight shift of the latter band to ~1572 cm^{-1}, as compared to that of the pristine CNTs. This is due to the sp^3-hybridized bonds and the influence of the functional groups present on the surface of the CNTs [44]. Accordingly, the D-to-G band (I_D/I_G) intensity ratio demonstrates the covalent sidewall derivation or introduction of defects into the CNTs [45]. Thus, the I_D/I_G value for both the primary (Cf-CNT) and secondary (Nf-, Sf-, Af-CNTs) functionalized CNTs were compared and were found to be 0.19-fold higher than that of the pristine CNTs, which reveals that it may possible to slightly disrupt the intrinsic conjugation during the functionalization process. Among the secondary functionalized samples, the Cf-CNTs exhibited the highest I_D/I_G value of 0.32. The I_D/I_G ratios of the Nf- and Sf-CNTs decreased to 0.16, whereas that of the Af-CNTs decreased even further to 0.13 after secondary functionalization. The decrease of I_D/I_G resulting from secondary surface functionalization of Cf-CNT to Nf-, Sf- and Af-CNT suggests a possible increase in the average size of the sp^2 domains [46]. Thus, the secondary functional groups of Nf-, Sf-CNTs linked by the amide bond where limited by the loading and location of carboxylic groups for Cf-CNTs [39]. In the case of Af-CNTs secondary functionalization was followed by the reaction with a carboxylic acid moiety allows direct attachment by the ester bond. Interestingly, the intensity of D-band decreased with conjugation of the AA units onto the primary functionalized CNTs given that sequential secondary functionalization of the Cf-CNTs to Af-CNTs does not induce further disorder of the CNT framework [47,48]. However, the increase in the I_D/I_G ratio for MWCNTs after decoration of Pt-nanoparticles by chemical reduction is an indication of nanoparticles incorporation over the surface of CNTs thereby creating defect sites or strong interaction of nanoparticles with Af-CNTs [49].

Structural data for the CNTs and functionalized CNTs were acquired using X-ray diffraction (XRD) (Fig. 2d). The diffraction pattern of the raw CNTs shows an intense peak at 26° corresponding to (002) plane, and minor peaks at 42.5° (100) and 53.5° (004); these peaks correspond to graphite in the sample. The XRD patterns of all the functionalized CNTs were identical to that of the raw CNT, except for the intensity of the peak at 26°. New and highly intense peaks were observed at 39.9°, 46.1°, and 67.9° for the metal-loaded Af-CNTs, ascribed to the platinum. The ternary Pt-Af-CNT/CdS hybrid material was compared with pure CdS, as shown in Fig. S2. No signals corresponding to graphite and Pt were observed in the diffraction pattern; this is expected due to the low content of these species in the composite CdS material. However, the presence of functionalized CNTs and Pt was further confirmed by compositional analysis via transmission electron microscopy-energy dispersive spectroscopy (TEM-EDS) and X-ray photoelectron spectroscopy (XPS).

2.4. Morphological analysis

Fig. 3 shows TEM images of the Pt-loaded Af-CNT/CdS nanohybrid. Notably, the walls of the Pt-loaded Af-CNTs showed high surface roughness, which may have resulted from the acid treatment during AA functionalization and Pt nanoparticle incorporation (Fig. 3a). Although TEM could not distinguish the minute functional groups, the surface deterioration of the CNTs that occurred as a result of functionalization was evident. The starting Pt nanoparticles with a size of 2–6 nm with few clusters were embedded on the surface of the Af-CNTs. It was

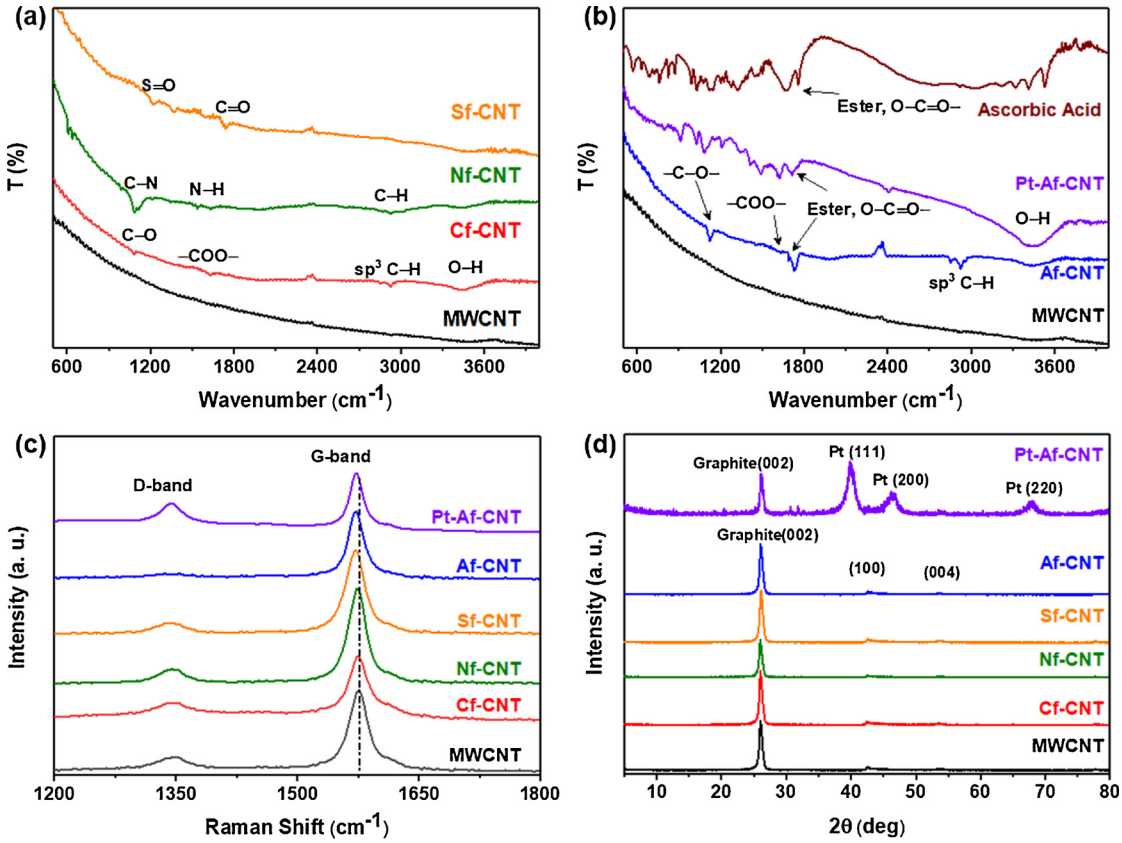

Fig. 2. FTIR spectrum of pristine MWCNT compared with functional groups presented in (a) Cf-CNT, Nf-CNT, Sf-CNT materials and, (b) Af-CNT, Pt-Af-CNT compared with pure ascorbic acid. (c) Raman spectra and (d) XRD pattern of pristine MWCNTs with primary and secondary functionalized CNTs compared with Pt nanoparticle-loaded Af-CNTs material.

confirmed that the Pt nanoparticles were well deposited on the functionalized CNTs, which may confer effective electron transfer characteristics to the composite. Fig. 3(b) shows that the Pt nanoparticle-loaded Af-CNTs were deposited on the surface of the approximately 30 nm diameter CdS nanorods. Fig. 3(b) inset show the SAED pattern marked with d-spacing of corresponding CdS, CNT and Pt in Pt-Af-CNT/CdS nanohybrid. As shown Fig. 3(c), the Pt-Af-CNTs were well dispersed and loaded on to the surface of the CdS nanorods, which should favor the surface shuttling between the CdS nanorods and Pt-Af-CNTs. The TEM images of pristine CNT, Af-CNT, CdS and SEM images of CNT,

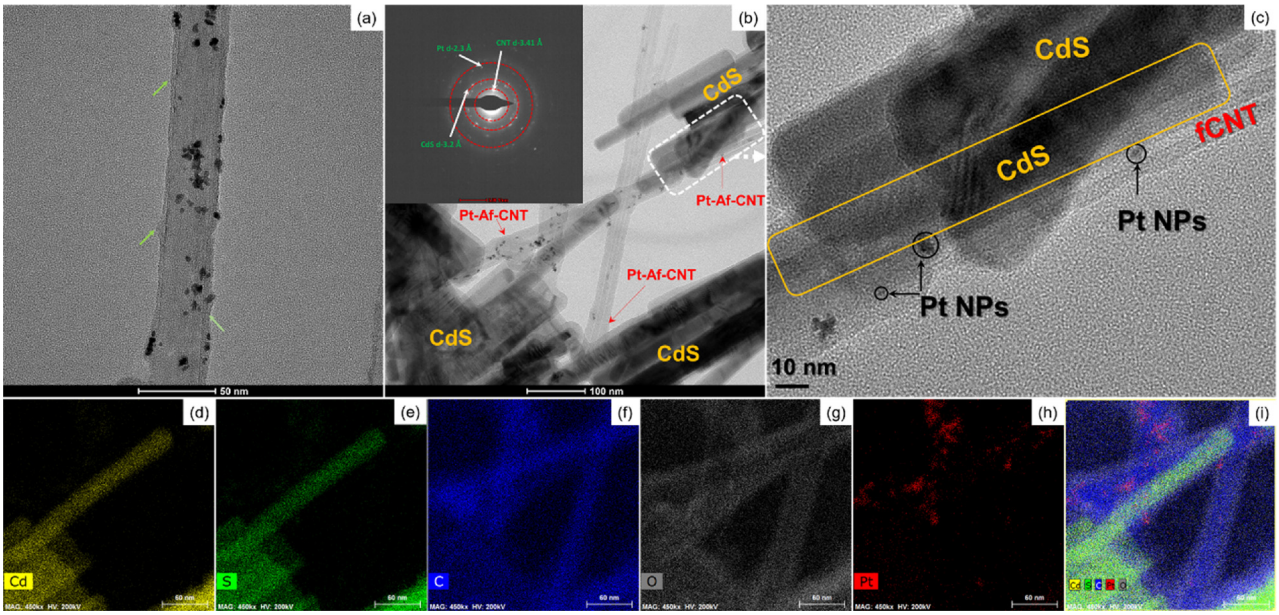

Fig. 3. TEM analysis of (a) Pt deposited on Af-CNTs; green arrows indicate the surface roughness caused by secondary AA functionalization. (b – c) Pt-Af-CNT/CdS ternary nanohybrid. Inset (b) show SAED pattern of Pt-Af-CNT nanohybrid, and (d – i) elemental analysis of the nanohybrid (Cd, S, C, O, and Pt). (For interpretation of the references to colour in this figure legend, the reader is referred to the web version of this article).

Pt-Af-CNT and Pt-Af-CNT/CdS has given in Fig S3. In addition, the Pt nanoparticles were finely deposited on the surface of the Af-CNTs, and this hybrid covered the CdS nanorods through the van der waals forces [34,50], influenced by the functional groups, affording surface contact between the Pt nanoparticles, Af-CNTs and CdS. The surface of the CdS nanorods in the Pt-Af-CNT/CdS nanohybrid were adequately crystalline, and the lattice spacing (3.2 Å) was well matched to the interplanar distance of the (101) plane of hexagonal CdS, as shown in Fig. 3(b) inset. Notably, optimizing the wt.% of the Pt-Af-CNTs, their adequate dispersion in water (as a solvent), and subsequent introduction of CdS leads to significant surface interfaces between these species. This superficial shuttling property of the Pt-Af-CNT/CdS nanohybrid is advantageous for charge transfer, separation, and enhancing the photoactivity for H_2 production.

The EDS mapping of elemental compositions for synthesized materials evaluated from the TEM image Fig. 3(b) by high magnification are displayed in Fig. 3(d)–(i). The results for the nanohybrid material confirm the presence of Cd, S, C, O, and Pt. Linear scanning elemental spectral analysis was also performed, as displayed in Fig. S4. Elemental mapping of O and Pt individually revealed the presence of O and Pt on the surface of the CNTs. It is indicative that AA functional groups are existed on all over CNTs and deposition of Pt nanoparticles on the CNTs surface and to be found beside the CdS nanorods. The EDS results are consistent with the XPS data, indicating successful functionalization with AA and deposition of the Pt nanoparticles on the CNT surface and interaction of this nanohybrid system with the CdS nanorods. The visible-light absorption ability of the as-synthesized nanocomposites (Cf-CNT/CdS, Af-CNT/CdS) and pure CdS nanorods were compared with that of the Pt-Af-CNT/CdS ternary nanohybrid (Fig. S5). The band-edge position of the pure CdS, binary Cf-CNT, Af-CNT nanocomposites, and ternary nanohybrids at 550 nm corresponds to a bandgap of 2.25 eV. However, the visible-light absorption capacity increased for both the binary and ternary nanohybrids due to the effective interactions caused by the deposited co-catalyst (Af-CNT and Pt). The calculated bandgaps of the nanocomposites and Pt-Af-CNT/CdS were almost similar to that of pure CdS. These results provide strong evidence that the binary nanocomposites and Pt-loaded ternary nanohybrids both have a higher capacity to utilize solar irradiation, which leads to an enhancement in the photocatalytic efficiency over that of the pure CdS nanorods.

2.5. Surface elemental analysis

The surface elemental composition and electronic structure of the Pt-loaded Af-CNT/CdS nanohybrid was analyzed by X-ray photoelectron spectroscopy (XPS). The XPS survey spectra of Pt-loaded Af-CNT/CdS and Cf-CNT/CdS nanohybrids were compared with pristine MWCNT and CdS, shown in Fig. S6 which confirm the presence of Cd, S, C, O, and Pt in ternary nanohybrids. Fig. 4(a) shows the deconvoluted C1s spectra of Pt-Af-CNT/CdS nanohybrid; the main peak located at 284.6 eV is ascribed to sp^2 hybridized carbon (C—C) in the CNTs [51]. The binding energy of the C1s peak at 286.5 eV corresponds to C—O (ether) or C=O (ketones and quinones) carbon [52]. The Af-CNT functional group characteristic peak at 289.0 eV binding energy was shifted from 288.5 eV binding energy (Cf-CNT functional group, shown in Fig. S6). This could be caused by the formation of the ester (O—CO) bond via the esterification reaction of AA on the surface of the CNTs [53]. In Fig. 4(a) inset show deconvoluted C1s spectra of pristine MWCNT, it is observable that there is no other peak that can represent the functional groups but the prominent binding energy (284.6 eV) of CNTs C—C Sp^2 hybridization. The deconvoluted O 1s and C 1s peaks are consistent with formation of the Cf-CNT and Af-CNT nanohybrids (Fig. S6) [47,54]. Thus, the secondary AA functional groups were linked to the carboxylic groups in the Cf-CNTs. The other peak at 283.7 eV is ascribed to C_2H_2/Pt or C_5H_{10}/Pt [54], and the presence of such hydrocarbons (C_xH_y) is likely due to chemical reduction with $NaBH_4$ while loading of the Pt nanoparticles onto the CNTs surface. The existence of the metallic form (Pt°) of the Pt nanoparticles was confirmed by the peaks at binding energies of 70.1 eV ($4f_{7/2}$) and 74.6 eV ($4f_{5/2}$) (Fig. 4(b)) [54]. Asymmetry was observed in the $4f_{5/2}$ level at ~78 eV, which may indicate a small population of PtO or PtO_2, which indicative of strong interaction of the Pt nanoparticles with the ester O from the Af-CNT functional groups [41]. Unfortunately, there was insufficient signal from the Pt oxide (PtO_x) to determine the relative stoichiometric proportions of the PtO and PtO_2 with precision. According to Hull et al., Pt nanoparticle deposition, finely dispersed clusters bind to the CNTs via bonding with ester and carbonyl O atoms [41]. The oxidation states of Cd and S were confirmed from the high-resolution XPS spectra presented in Fig. 4(c) and (d). The Cd 3d peaks at binding energies of 405.1 eV and 411.9 eV correspond to the $Cd3d_{5/2}$ and $Cd3d_{3/2}$ states, respectively. This result confirms that Cd is in the +2 oxidation state in CdS and the pristine CdS expanded Cd 3d and S 2p has shown in Fig. S6(e) and (f). Moreover, the two apparent main peaks at 161.2 eV and 162.5 eV are assigned to S^{2-} (S $2p_{3/2}$) in CdS [55]. The XPS results strongly confirm successful secondary functionalization and formation of the Pt-Af-CNT nanohybrid.

2.6. Photoluminescence spectral analysis

Fig. 4(e) shows the PL spectra of the pure CdS nanorods, binary Cf-, Af-CNT/CdS, and ternary Pt-loaded nanohybrids. The PL spectra of the binary Cf-, Af-CNT/CdS, and their Pt-loaded ternary nanohybrids showed low-intensity emission and a slight blue-shift of the primary peak of CdS, which corresponds to the band-edge emission. The weak emission bands indicate that most of the surface states were passivated, making the electrons available for photocatalytic H_2 evolution. It can be deduced that the surface-modified and Pt-loaded CNTs have a stronger impact on CdS and more photogenerated electrons become involved in reducing H^+ to H_2, which reduces recombination. A similar quenching of the PL emission has previously been reported [56,57], and was ascribed to effective electron transfer from the semiconductor to CNTs and/or metal nanoparticles, which facilitated effective separation of the photo-induced electron-hole pairs.

2.7. Photoelectrochemical (PEC) analysis

The separation efficiency and photo-induced charge carrier transport were photoelectrochemically examined under simulated solar-light irradiation using indium tin oxide (ITO) electrodes coated with CdS, binary Cf-, the Af-CNT/CdS nanocomposites, Pt nanoparticle-loaded Cf-, and Af-CNT/CdS nanohybrids as displayed in Fig. 4(f). The transient photocurrent response data for five consequent on/off irradiation cycles of 30 s intervals. The Af-CNT/CdS composite produced a stronger photocurrent than pristine CdS and Cf-CNT/CdS; thus, the ternary Pt-Af-CNT/CdS nanohybrid significantly enhanced generation of the photocurrent, with a value of around 3.6 μA in 30 s. Similar results have been reported by Kim et al. [33] using Pt loaded on traditional acid-functionalized CNT/CdS; however, we compared the results with those obtained with the as-synthesized Cf-CNTs and Pt loaded Cf-CNTs on the CdS nanohybrid and observed a lower photocurrent than obtained with Pt-Af-CNT/CdS. The higher photocurrent observed with the latter may be attributed not only to the increased purity of the CNTs, but also to the presence of the Pt catalyst that was strongly bound to the Af-CNT surface. This higher photocurrent demonstrates the important synergistic effect of the catalyst on the Af-CNT surface and suggests a higher separation efficiency of the photoexcited e^+/h^+ pairs and consequent improvement in the proton reduction, leading to enhanced H_2 production. The photocurrent responses were highly reproducible and remained stable for several on-off cycles, indicating that both the Af-CNT/CdS nanocomposite and Pt-Af-CNT/CdS nanohybrids can effectively resist photocorrosion. These photocurrent measurements are consistent with the PL spectral data. In addition, the electrochemical

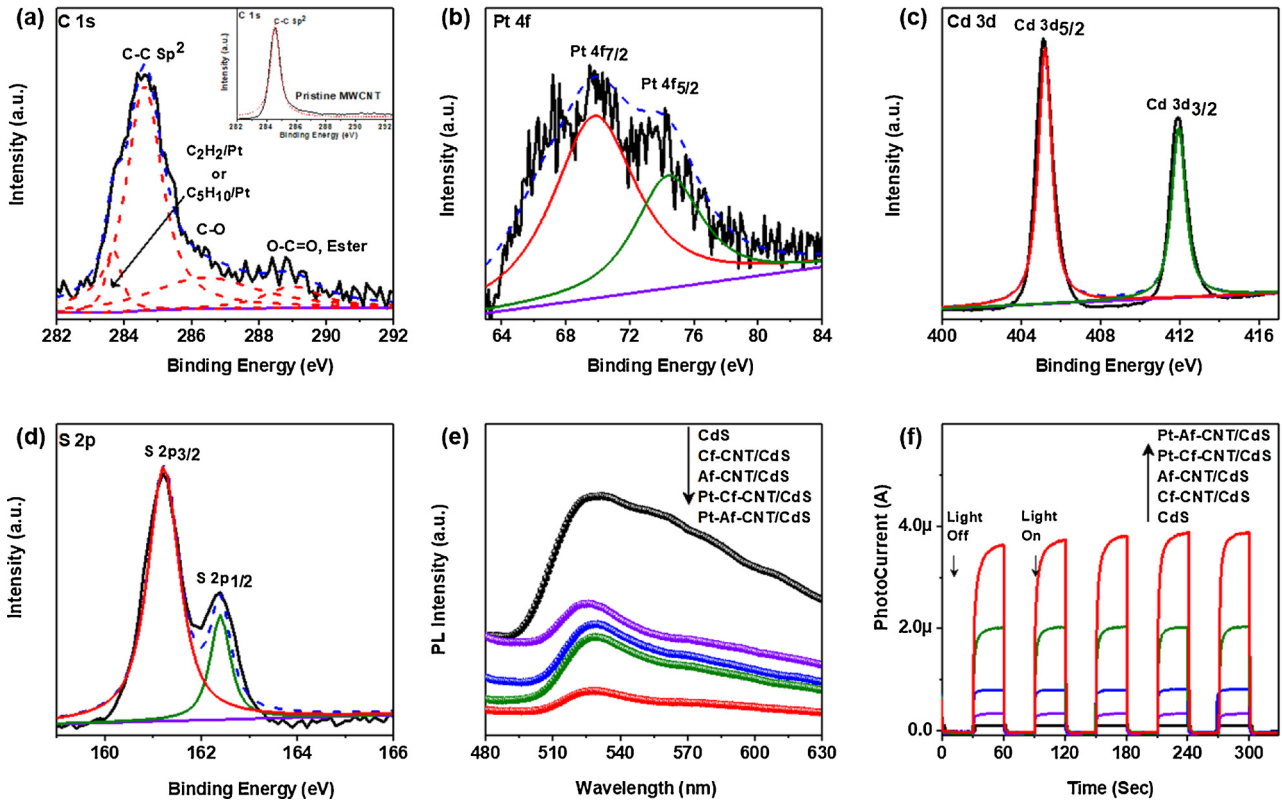

Fig. 4. X-ray photoelectron spectra of Pt-Af-CNT/CdS composite showing expanded (a) C 1s and (inset show pristine MWCNT expanded C1s), (b) Pt 4f, (c) Cd 3d and (d) S 2p spectral regions. (e) Photoluminescence (PL) analysis and (f) photoelectrochemical (PEC) analysis of pure CdS, binary Cf-CNT, Af-CNT on CdS, and ternary Pt-Cf-CNT and Pt-Af-CNT on CdS nanorods.

impedance spectroscopy (EIS) result in Fig. S7 shows a typical semicircles at high frequencies for binary Af-CNT/CdS and Pt-Af-CNT/CdS ternary nanocomposites than pristine CdS and traditional primary functionalized Cf-CNT/CdS nanocomposite, suggesting the faster interfacial charge transfer of secondary functionalized Pt-Af-CNT/CdS. Thus, evaluating the effect of the surface interactions of functionalized CNTs and their role in water splitting via photocatalytic activity studies remains a fascinating task.

2.8. Photocatalytic activity

2.8.1. Effect of surface modified CNTs and metal nanoparticles on CdS nanorods

First, deposition of the functionalized CNTs was optimized by varying the loading (0 − 10 wt.%) of Cf-CNTs on the CdS nanorods and applying the products to photocatalytic H_2 production studies using 20 vol.% of lactic acid aqueous solution under simulated solar-light irradiation. Fig. 5(a) shows the amount of H_2 produced as a function of the Cf-CNT loading on the CdS nanorods; the composite catalysts showed a significant rate of H_2 generation relative to pure CdS. In the presence of the functionalized CNTs, the CdS photocatalyst led to an improved rate of H_2 production with increasing amounts of Cf-CNT up to an optimal level of 6 wt.%; the same loading was used for the secondary functionalized Nf-, Sf-, and Af-CNTs, and for Pt-Af-CNT on the surface of the CdS nanorods. Further loading of the functionalized CNTs onto CdS led to a reduction in the H_2 production rate. Fig. 5(b) shows that the photocatalytic H_2 production activities of all surface-functionalized CNT/CdS composites were improved relative to that of the pure CdS nanorods (2.5 mmol h^{-1} g^{-1})[1] under simulated solar-light irradiation. The functional groups introduced onto the CNTs produced a synergetic effect when placed on the CdS surface, where the activity increased to 6.1 mmol h^{-1} g^{-1} for the Cf-CNT/CdS nanocomposite. In the case of Af-CNT/CdS, the H_2 production increased significantly to 16.7 mmol h^{-1} g^{-1}, which is about six times that of pure CdS. To confirm the reproducibility of H_2 production with the Af-CNT/CdS catalyst, the experiment was repeated five times and almost identical results were obtained (Fig. S8). Furthermore, we studied the effects of a sacrificial agent, the concentration of the sacrificial agent, and the photocatalyst loading on the photocatalytic H_2 production; relevant results are presented in Fig. S8. The Nf- and Sf-CNT/CdS composites produced improved activity relative to that of pure CdS and the Cf-CNTs; however, for the Nf- and Sf-CNTs, the H_2 production rate was not higher than that of the AA-functionalized CNT nanocomposite. This clearly illustrates the importance of functional groups on the surface-treated CNTs in influencing H_2 production by photocatalytic water splitting.

Further, to improve the photocatalytic H_2 production rate, the Af-CNT/CdS nanocomposite metal nanoparticles were loaded onto Af-CNT using the consecutive adsorption and chemical reduction process; the CdS nanorods were then immobilized on the metal nanoparticle-loaded Af-CNTs (M-Af-CNT/CdS). Fig. 5(d) shows that for the M-Af-CNT/CdS (M: Pt, Ru, Pd, Ni, Ag, and Cu) nanohybrids, a maximum H_2 production of 120.1 mmol h^{-1} g^{-1} under 3 h of solar light irradiation was achieved with the Pt-loaded Af-CNT/CdS. This greater H_2 production indicates that functionalization of the CNTs with AA provides numerous binding sites for the Pt cations (Pt^{2+}) and significant surface interactions with CdS. The photocatalytic H_2 production performance of the metal nanoparticle-loaded Af-CNT/CdS hybrid suspensions followed the order: Pt > Ru > Pd > Ni > Ag > Cu, as shown in Fig. 5(d). In general, Pt is known to be the best proton reduction co-catalyst in semiconductor photocatalysis in relation to other metal nanoparticles such as Ru, Pd, Ni, Ag, and Cu, and is thus the most widely used catalyst in CdS-based photocatalytic H_2 production [58]. The results obtained herein demonstrate that the prepared nanohybrids and their ability for

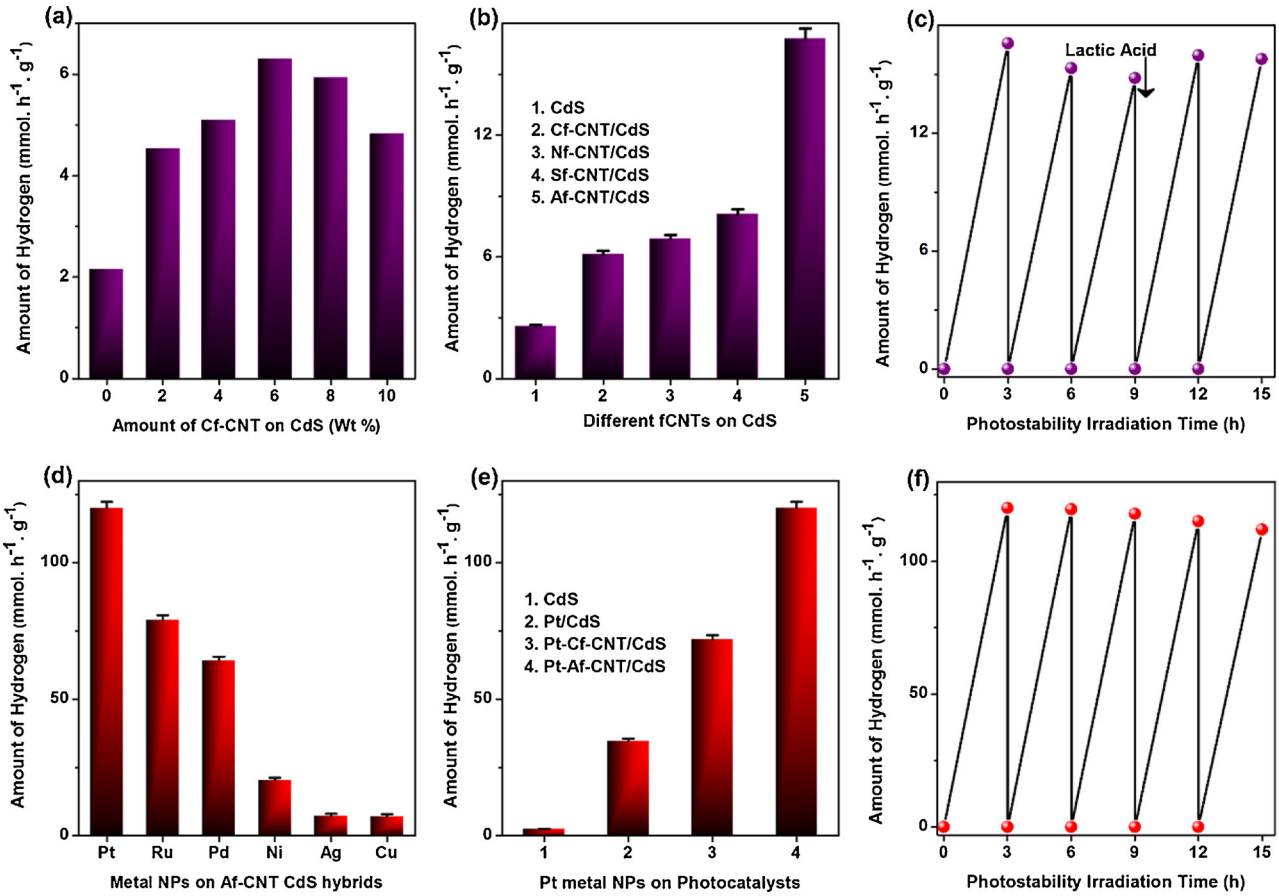

Fig. 5. (a) Optimization of Cf-CNT loading on CdS nanorods. (b) Comparison of hydrogen production with secondary functionalized CNTs on CdS nanocomposites. (d) Effect of metal nanoparticles on Af-CNTs versus CdS nanohybrid on hydrogen production. (e) Comparison of hydrogen production with Pt nanoparticle-loaded materials versus pure CdS. Photostability of binary Af-CNT/CdS nanocomposite (c) and ternary Pt-Af-CNT/CdS nanohybrid (f).

surface shuttling from CdS to the CNTs and metal nanoparticles could enhance the catalytic water splitting reactions and thus enhance H_2 production under solar-light irradiation.

Fig. 5(e) shows a comparison of the amount of hydrogen produced by the Pt nanoparticle-coupled surface functionalized Af-CNTs and Cf-CNT nanohybrids versus Pt-CdS and pure CdS. Approximately 120.1 mmol h^{-1} g^{-1} of H_2 was produced with the Pt-Af-CNTs/CdS hybrid, which is higher than that produced with the Pt-Cf-CNT/CdS nanohybrid (72 mmol h^{-1} g^{-1}). The additional functional groups act as surface active sites for the Af-CNTs relative to the Cf-CNTs, which should influence H_2 production via photo-induced water splitting. As shown in Fig. 5(e), the activity of the Pt-Af-CNT/CdS hybrid photocatalyst was enhanced by about 48- and 3.5-fold compared to that of pure CdS and the Pt/CdS nanocomposite, respectively. This superior H_2 production was observed due to the influence of deposition of the Pt nanoparticles on the AA-functionalized CNTs and the interaction of this hybrid with the surface of the CdS nanorods. Thus, this Pt-Af-CNT/CdS hybrid system should enhance the e-/h^+ pair separation by charge transport and retard the recombination process; these expectations are well supported by the PL and photocurrent measurements.

2.8.2. Photostability and durability measurements

The binary Af-CNT/CdS composite material and ternary Pt-Af-CNT/CdS nanohybrid were both further subjected to photostability experiments. Fig. 5(c) and (f) clearly show that the nanohybrid was more stable and was reusable for several cycles. An identical amount of H_2 was produced for five successive experiments, although a slight decrease was observed for the binary composite during the third cycle, as shown in Fig. 5(c). This may be attributed to the oxidation of lactic acid during the photocatalytic reaction, as confirmed by the pH of the reaction solution before and after the photoexperiments [59]. The concentration of the sacrificial agent was decreased by (water, lactic acid, or its intermediates) consuming photogenerated holes in the valence bands (VB) of CdS, which led to the generation of protons and intermediates. Zhang et al. [60] reported that the formation of oxidized intermediates from lactic acid (to pyruvic acid) after the photocatalytic process led to a difference in the pH of the reaction solutions before and after the reactions. Additional lactic acid was added to the photoreactor, and in the fourth and fifth cycles, the H_2 evolution rate was recovered to that of the first and second cycles. This result demonstrates that continuous H_2 evolution is mainly dependent on the availability of a hole sacrificial agent in the reaction medium. The Pt-loaded ternary nanohybrid was the most stable material and an identical amount of H_2 was produced in three consequent cycles; a minor decrease in activity was observed in the fifth and sixth cycles (Fig. 5(f)).

Fig. 6(a) shows the time-course for photocatalytic H_2 evolution over Pt-Af-CNTs/CdS, Af-CNT/CdS, and pure CdS under visible-light and full spectrum irradiation by a Xe lamp. As can be seen in Fig. 6(a), Pt-Af-CNTs/CdS showed much higher photoactivity than the composites and pure CdS. Under visible-light irradiation, the total amount of H_2 produced increased in the order: Pt-Af-CNT/CdS > Af-CNT/CdS > pure CdS for the first 3 h of the photoreaction.

In addition, the apparent quantum efficiencies (QEs) of the pure CdS, Af-CNT/CdS composite, and Pt-Af-CNT/CdS nanohybrid were determined by quantifying the amount of H_2 produced at a given photon flux, as summarized in Table 1. The QE (29.1%) and the photocatalytic H_2 production (120.1 mmol h^{-1} g^{-1}) were highest for the Pt-Af-CNT/CdS nanohybrid, which was the most efficient material

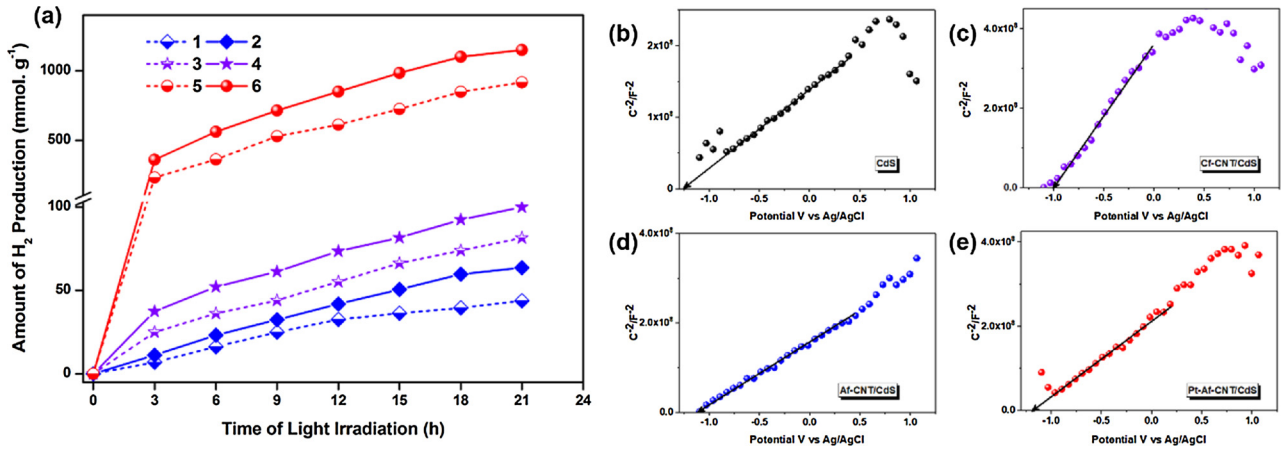

Fig. 6. (a) Time-profile for H_2 evolution by photocatalytic water splitting under visible light (dotted lines) and full solar spectrum (solid lines) irradiation using pure CdS (blue 1 – 2), binary Af-CNT/CdS (violet 3 – 4), and ternary Pt loaded Af-CNT/CdS (red 5 – 6). (b–e) Mott-Schottky measurements for pristine CdS, binary Cf-CNT/CdS, Af-CNT/CdS and ternary Pt-loaded Af-CNT/CdS (For interpretation of the references to colour in this figure legend, the reader is referred to the web version of this article).

Table 1
Photocatalytic hydrogen production by functionalized CNT nanohybrids under solar light. QEs (%) were calculated for pure CdS, Af-CNT/CdS, and Pt-Af-CNT/CdS under visible light (≥ 425 nm) irradiation.

Photocatalyst	H_2 Production Rate(mmol h^{-1} g^{-1})	AQE %(λ ≥ 425 nm)
CdS	2.57	0.88
Cf-CNT/CdS	6.1	
Nf-CNT/CdS	6.8	
Sf-CNT/CdS	8.1	
Af-CNT/CdS	16.7	3.3
Pt/CdS	34.9	
Pt-Cf-CNT/CdS	72	
Pt-Af-CNT/CdS	120.1	29.1
Ru-Af-CNT/CdS	79	
Pd-Af-CNT/CdS	64	
Ni-Af-CNT/CdS	20	
Ag-Af-CNT/CdS	7.4	
Cu-Af-CNT/CdS	7.3	

based on comparison with earlier reports (Table S1). In the case of the CdS nanorods and Af-CNT/CdS nanocomposite, the QEs were about 0.88 and 3.3%, respectively. Moreover, full spectrum irradiation significantly increased the amount of H_2 produced with the same materials. Both visible light and full spectrum irradiation were continued for up to 21 h for the long-term photostability experiments. The results indicated that the prepared nanocomposite and ternary nanohybrids were robust and stable photocatalysts for H_2 production. To verify the structural stability of Pt-Af-CNT/CdS after the recycling measurements, XRD, XPS, and TEM analyses were performed and the obtained results are presented in Fig. S9; there were no structural or chemical composition changes after recycling, which indicates that the synthesized hybrid is the most stable and efficient of the catalysts for photocatalytic H_2 production.

2.8.3. Proposed reaction mechanism

A plausible mechanism for the efficient H_2 production under solar-light irradiation with lactic acid as a hole scavenger and Pt-Af-CNT/CdS as a photocatalyst is depicted in Scheme 1. Under solar-light irradiation, semiconducting CdS in the Pt-Af-CNT/CdS nanohybrid should excite the electrons to the conduction band, leaving holes in the valance band [60,61]. To confirm the exact conduction band (CB) potential of the pristine CdS, Cf-CNT/CdS, Af-CNT/CdS and Pt-Af-CNT/CdS samples, we carried out Mott–Schottky (MS) measurements to understand the mechanism of photocatalytic hydrogen production, which are shown in Fig. 6(b)–(e). The flat band potentials of the samples were estimated approximately equal to −1.24 V, −1.0 V, −1.1 V, and −1.17 V *vs.* Ag/AgCl for pristine CdS, Cf-CNT /CdS, Af-CNT/CdS and Pt-loaded Af-CNT/CdS, respectively. The CB potentials vs. Ag/AgCl were converted to the normal hydrogen electrode (NHE) scale by $E_{NHE} = E_{Ag/AgCl} + 0.197$ V at pH 7, and the converted values are −0.94, −0.703, −0.81, and −0.89 V (vs. E_{NHE}) for CdS, Cf-CNT /CdS, Af-CNT/CdS and Pt-loaded Af-CNT/CdS, respectively. The CB potential of the functionalized CNT/CdS binary nanocomposites are positive than that of CdS and more negative than the H^+ reduction potentials (−0.410 V vs. E_{NHE} at pH 7) [62]. Furthermore, the CB potential of Pt-Af-CNT/CdS nanohybrid is much closer to that of CdS than that of Af-CNT/CdS. Thus, excited electrons on CdS can transfer to Pt-loaded Af-CNT more efficiently than to Af-CNT, increasing the possibility of hydrogen production. The functionalized CNTs play a multi-functional role as a dispersant in the aqueous solvent and as a supporting material and electron acceptor to improve the surface e^-/h^+ pair separation and shuttling; this reduces recombination in CdS and improves the efficiency of the nanohybrid system. The photo-induced excited electrons migrate in three pathways to improve the H^+/H_2 reduction reaction. In the first, the excited electron is transferred to the CNTs and effectively separates the photogenerated holes, followed by reduction [63]. The second pathway features the transfer of the excited electrons to the Pt nanoparticles and separation of the photogenerated charge carriers, followed by reduction, given that the Pt nanoparticles dispersed all over the CNT surfaces could also interact with the CdS surface. Finally, the excited electrons could be transferred to the Pt nanoparticles via the CNTs, which effectively separates the charge carriers and improves the surface shuttling ability, followed by reduction of the protons to increase the H_2 production. The CNTs should enable the transfer of excited electrons from CdS to the catalytically active Pt nanoparticles. Furthermore, the hydrophilicity of the AA functional groups on the CNTs counteracts the hydrophobicity of the CNTs, which favors water adsorption/dissociation equilibria and proton translocation steps. The sacrificial agent (i.e., lactic acid) is oxidized by the photogenerated holes in the VB of the CdS. However, the Af-CNT/CdS composite and Pt-Af-CNT/CdS nanohybrid exhibited superior activity compared to the traditional acid-functionalized Cf-CNT/CdS composites. Building on existing concepts, a combination of AA-functionalized CNTs and Pt nanoparticles that were integrated on the surface of CdS nanorods are reported herein for the first time. The resulting nanocomposite provides organization of the metal oxide, nanocarbon, and metal nanoparticle interfaces, where the specific characters of the individual components merge to induce astonishing photocatalytic water-splitting H_2 production. Present structural, optical, and photo-electrochemical results

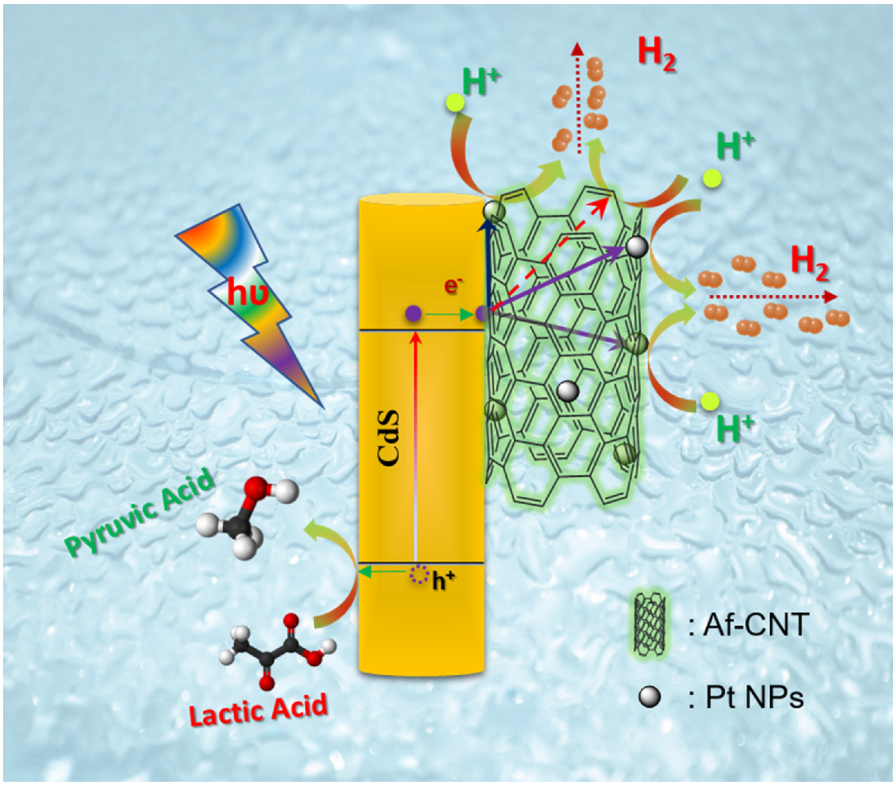

Scheme 1. Mechanism of H_2 production via photocatalytic water splitting by Pt-Af-CNT/CdS ternary nanohybrid.

supports the proposed reaction mechanism.

3. Conclusion

In conclusion, the nanohybrids of CdS and surface-modified CNTs, developed herein function as effective light-harvesting materials. The novel approach of employing the AA functionalized CNTs leads to the dual role of a supporting semiconductor photocatalyst and metal catalyst, and assists with catalyzing proton/water reduction. Conversely, the performance of the nanohybrid is very sensitive to the surface-treatment of the CNTs, given that the properties of the CNTs are critically dependent on their surface states. This indicates that non-cautious treatment of CNTs can minimize or even nullify the effects of the CNTs, even when highly efficient photocatalysts and other catalysts are employed. Therefore, the surface treatment of the CNTs must be carefully selected and performed, and the energetics, electrostatics, etc., of the CNTs, photocatalyst, and co-catalyst must be carefully matched to obtain enhanced photocatalytic efficiency. This scheme is expected to provide insight into the photocatalytic and electrocatalytic mechanisms while providing a versatile and flexible catalyst platform for a sustainable energy and environmental economy.

Acknowledgements

This work was supported by National Research Foundation of Korea (NRF) grants, funded by the Korean Government (2014R1A4A1001690, 2016K1A4A4A01922028 and 2016R1E1A1A01941978).

Appendix A. Supplementary data

Supplementary material related to this article can be found, in the online version, at doi: https://doi.org/10.1016/j.apcatb.2018.05.009.

References

[1] S. Iijima, Nature 354 (1991) 56–58.
[2] C.J. Shearer, A. Cherevan, D. Eder, Adv. Mater. 26 (2014) 2295–2318.
[3] R. Leary, A. Westwood, Carbon 49 (2011) 741–772.
[4] P.M. Ajayan, Chem. Rev. 99 (1999) 1787–1800.
[5] R.H. Baughman, A.A. Zakhidov, W.A. de Heer, Science 297 (2002) 787–792.
[6] A. Le Goff, V. Artero, B. Jousselme, P.D. Tran, N. Guillet, R. Métayé, A. Fihri, S. Palacin, M. Fontecave, Science 326 (2009) 1384–1387.
[7] D.R. Kauffman, A. Star, Angew. Chem. Int. Ed. 47 (2008) 6550–6570.
[8] M. Gopannagari, H. Chaturvedi, Nanoscale 7 (2015) 16590–16596.
[9] N. Karousis, N. Tagmatarchis, D. Tasis, Chem. Rev. 110 (2010) 5366–5397.
[10] D.M. Guldi, G. Rahman, F. Zerbetto, M. Prato, Acc. Chem. Res. 38 (2005) 871–878.
[11] G. Ovejero, J.L. Sotelo, M.D. Romero, A. Rodríguez, M.A. Ocaña, G. Rodríguez, J. García, Ind. Eng. Chem. Res. 45 (2006) 2206–2212.
[12] C. Chen, B. Liang, A. Ogino, X. Wang, M. Nagatsu, J. Phys. Chem. C 113 (2009) 7659–7665.
[13] Y.-P. Sun, K. Fu, Y. Lin, W. Huang, Acc. Chem. Res. 35 (2002) 1096–1104.
[14] N.P. Blanchard, R.A. Hatton, S.R.P. Silva, Chem. Phy. Lett. 434 (2007) 92–95.
[15] L. Wang, Z. Yao, F. Jia, B. Chen, Z. Jiang, Dalton Trans. 42 (2013) 9976–9981.
[16] T. Peng, P. Zeng, D. Ke, X. Liu, X. Zhang, Energy Fuels 25 (2011) 2203–2210.
[17] A. Ye, W. Fan, Q. Zhang, W. Deng, Y. Wang, Catal. Sci. Technol. 2 (2012) 969–978.
[18] K. Dai, T. Peng, D. Ke, B. Wei, Nanotechnology 20 (2009) 125603.
[19] V.T. Le, C.L. Ngo, Q.T. Le, T.T. Ngo, D.N. Nguyen, M.T. Vu, Adv. Nat. Sci. 4 (2013) 035017.
[20] G. Valenti, A. Boni, M. Melchionna, M. Cargnello, L. Nasi, G. Bertoni, R.J. Gorte, M. Marcaccio, S. Rapino, M. Bonchio, P. Fornasiero, M. Prato, F. Paolucci, Nat. Commun. 7 (2016) 13549.
[21] S. Mallakpour, S. Rashidimoghadam, Carbohydr. Polym. 169 (2017) 23–32.
[22] C. Hu, Y. Zhang, G. Bao, Y. Zhang, M. Liu, Z.L. Wang, J. Phys. Chem. B 109 (2005) 20072–20076.
[23] D. Tasis, N. Tagmatarchis, A. Bianco, M. Prato, Chem. Rev. 106 (2006) 1105–1136.
[24] M.T. Byrne, Y.K. Gun'ko, Adv. Mater. 22 (2010) 1672–1688.
[25] C. Klinke, J.B. Hannon, A. Afzali, P. Avouris, Nano Lett. 6 (2006) 906–910.
[26] P. Singh, S. Campidelli, S. Giordani, D. Bonifazi, A. Bianco, M. Prato, Chem. Soc. Rev. 38 (2009) 2214–2230.
[27] L.-L. Ma, H.-Z. Sun, Y.-G. Zhang, Y.-L. Lin, J.-L. Li, E.-k. Wang, Y. Yu, M. Tan, J.-B. Wang, Nanotechnology 19 (2008) 115709.
[28] M.M. Kumari, D.P. Kumar, P. Haridoss, V.D. Kumari, M. Shankar, Int. J. Hydrogen Energy 40 (2015) 1665–1674.
[29] X. Lu, W.-L. Yim, B.H.R. Suryanto, C. Zhao, J. Am. Chem. Soc. 137 (2015) 2901–2907.
[30] R. Marschall, Adv. Funct. Mater. 24 (2014) 2421–2440.
[31] I. Robel, B.A. Bunker, P.V. Kamat, Adv. Mater. 17 (2005) 2458–2463.
[32] J. Cao, J.Z. Sun, J. Hong, H.Y. Li, H.Z. Chen, M. Wang, Adv. Mater. 16 (2004)

84–87.
[33] Y.K. Kim, H. Park, Energy Environ. Sci. 4 (2011) 685–694.
[34] M.M.-J. Li, P. Mills, S.M. Fairclough, A. Robertson, Y.-K. Peng, J. Warner, C. Nie, E. Flahaut, S.C.E. Tsang, Chem. Comm. 52 (2016) 13596–13599.
[35] J. Feng, G. Liu, S. Yuan, Y. Ma, Phys. Chem. Chem. Phys. 19 (2017) 4997–5003.
[36] Q. Mu, W. Liu, Y. Xing, H. Zhou, Z. Li, Y. Zhang, L. Ji, F. Wang, Z. Si, B. Zhang, B. Yan, J. Phys. Chem. C 112 (2008) 3300–3307.
[37] N. Smirnoff, G.L. Wheeler, Crit. Rev. Biochem. Mol. Biol. 35 (2000) 291–314.
[38] S. Mallakpour, A. Zadehnazari, J. Solid State Chem. 211 (2014) 136–145.
[39] S.K. Park, Q. Mahmood, H.S. Park, Nanoscale 5 (2013) 12304–12309.
[40] H.-J. Lee, S.-J. Oh, J.-Y. Choi, J.W. Kim, J. Han, L.-S. Tan, J.-B. Baek, Chem. Mater. 17 (2005) 5057–5064.
[41] R.V. Hull, L. Li, Y. Xing, C.C. Chusuei, Chem. Mater. 18 (2006) 1780–1788.
[42] B.P. Vinayan, R. Nagar, V. Raman, N. Rajalakshmi, K.S. Dhathathreyan, S. Ramaprabhu, J. Mater. Chem. 22 (2012) 9949–9956.
[43] U.J. Kim, C.A. Furtado, X. Liu, G. Chen, P.C. Eklund, J. Am. Chem. Soc. 127 (2005) 15437–15445.
[44] D.-Q. Yang, J.-F. Rochette, E. Sacher, J. Phys. Chem. B 109 (2005) 7788–7794.
[45] H.S. Park, B.G. Choi, W.H. Hong, S.-Y. Jang, J. Phys. Chem. C 116 (2012) 7962–7967.
[46] M.K. Shin, B. Lee, S.H. Kim, J.A. Lee, G.M. Spinks, S. Gambhir, G.G. Wallace, M.E. Kozlov, R.H. Baughman, S.J. Kim, Nat. Comm. 3 (2012) 650.
[47] D.D. Chronopoulos, C.G. Kokotos, N. Karousis, G. Kokotos, N. Tagmatarchis, Nanoscale 7 (2015) 2750–2757.
[48] C.A.C.- Roldán, G.R.- Sánchez, R.G.G.- Huerta, J.R.V. Garcia, P.B. Balbuena, N.A. Vante, ACS Appl. Mater. Interfaces 8 (2016) 23260–23269.
[49] M. Baro, P. Nayak, T.T. Babya, S. Ramaprabhua, J. Mater. Chem. A 1 (2013) 482–486.
[50] J.N. Coleman1, M. Lotya, A. O'Neill1, S.D. Bergin, P.J. King, U. Khan, K. Young, A. Gaucher, S. De, R.J. Smith, I.V. Shvets, S.K. Arora, G. Stanton, H.Y. Kim, K. Lee, G.T. Kim, G.S. Duesberg, T. Hallam, J.J. Boland, J.J. Wang, J.F. Donegan, J.C. Grunlan, G. Moriarty, A. Shmeliov, R.J. Nicholls, J.M. Perkins, E.M. Grieveson, K. Theuwissen, D.W. McComb, P.D. Nellist, V. Nicolosi, Science 331 (2011) 568–571.
[51] T.I.T. Okpalugo, P. Papakonstantinou, H. Murphy, J. McLaughlin, N.M.D. Brown, Carbon 43 (2005) 153–161.
[52] S. Kundu, Y. Wang, W. Xia, M. Muhler, J. Phys. Chem. C 112 (2008) 16869–16878.
[53] W. Francisco, F.V. Ferreira, E.V. Ferreira, Ld.S. Cividanes, Ad.R. Coutinho, G.P. Thim, J. Aerosp. Technol. Manage. 7 (2015) 289–293.
[54] A.V. Naumkin, A. Kraut-Vass, S.W. Gaarenstroom, C.J. Powell, NIST Standard Reference Database 20, Version 4.1, (2017) (accessed 20 December 2017), http://srdata.nist.gov/xps/Default.aspx.
[55] D.A. Reddy, H. Park, R. Ma, D.P. Kumar, M. Lim, T.K. Kim, ChemSusChem 10 (2017) 1563–1570.
[56] D.P. Kumar, S. Hong, D.A. Reddy, T.K. Kim, Appl. Catal. B Environ. 212 (2017) 7–14.
[57] S. Han, L. Hu, N. Gao, A.A. Al-Ghamdi, X. Fang, Adv. Funct. Mater. 24 (2014) 3725–3733.
[58] J. Yang, D. Wang, H. Han, C. Li, Acc. Chem. Res. 46 (2013) 1900–1909.
[59] D.P. Kumar, J. Choi, S. Hong, D.A. Reddy, S. Lee, T.K. Kim, A.C.S. Sustain, Chem. Eng. 4 (2016) 7158–7166.
[60] W. Zhang, Y. Wang, Z. Wang, Z. Zhong, R. Xu, Chem. Comm. 46 (2010) 7631–7633.
[61] B. Qiu, Q. Zhu, M. Xing, J. Zhang, Chem. Comm. 53 (2017) 897–900.
[62] Q. Xiang, B. Cheng, J. Yu, Angew. Chem. Int. Ed. 54 (2015) 11350–11366.
[63] J. Yu, B. Yang, B. Cheng, Nanoscale 4 (2012) 2670–2677.